CHAPTER IV
PREVULCANIZED NATURAL RUBBER LATEX/CLAY AEROGEL NANOCOMPOSITES

4.1 Abstract

Natural rubber latex (NR)/clay aerogel nanocomposites were produced via freeze-drying technique. The pristine clay (sodium montmorillonite) was introduced in 1, 2, and 3 parts per hundred rubber (phr) in order to study the effect of clay in the NR matrix. The dispersion of the layered clay and the morphology of the nanocomposites were determined by X-ray diffraction (XRD) and scanning electron microscopy (SEM), respectively. Cure characteristics, thermal stability, and the crosslink density of thermal and microwave-cured NR and its composites were investigated. XRD patterns indicated that both intercalated and exfoliated structures were observed at loadings of 1 to 3 phr clay. SEM studies revealed that the clay aerogel structure was formed at 3 phr clay loading. The increment in Shore A hardness of nanocomposites compared with pure NR signified excellent polymer/filler interaction and the reinforcing effect of the clay to rubber matrix. This was supported by an increase in maximum rheometric torque and crosslink density. The crosslink density of clay-filled NR vulcanizates was found to increase with the pristine clay content in both thermal and microwave curing methods. However, microwave-cured 2 and 3 phr-filled NR vulcanizates exhibited higher crosslink density than those which were thermal cured under the same curing temperature. In addition, thermal stability studies showed that pristine clay accelerated the decomposition of NR by showing a slight decrease in onset and peak decomposition temperatures along with clay content.

Keywords: Prevulcanized natural rubber latex; Clay aerogel; Nanocomposites; Crosslink density

4.2 Introduction

Nanocomposites are materials that have a nanometer scale dispersion of reinforcing agents (at least in one dimension) [1]. Clay and clay minerals, such as sodium montmorillonite, saponite, hectorite, bentonite, etc., have been widely used as natural fillers in making the nanocomposites. Not only has the development of polymer–clay nanocomposites gained a lot of interest in recent years, but developments in natural rubber–clay nanocomposites have also captured the eyes of many researchers. The main reasons for adding clay fillers to rubber are to enhance the mechanical properties and to make the final products less expensive. The ability of layered silicates to separate into individual layers with a very high aspect ratio (high length-to-width ratio) and to undergo ion-exchange reactions with inorganic or organic cations are general concerns in making rubber–clay nanocomposites. These factors have led to the enhancement in hardness, modulus, tensile and tear strength, thermal stability, fatigue resistance, and the gas barrier properties of NR nanocomposites [2-7]. Recently, Stephen, R. *et al.* [8] reported that the high aspect ratio of layered silicates not only provided reinforcement of nanocomposites but also lowered the gas permeability through the layered silicate reinforced latex membranes, whereas micro-filled composites provided higher gas permeability. Normally, the methods for preparing natural rubber-based nanocomposites are co-coagulating, in situ polymerization, melt intercalation, and latex compounding. In situ polymerization and melt intercalation are processes in which an organoclay must be employed [1, 6], while the others require only pristine clay [2-5, 7]. The structure of nanocomposites can be classified into two types: intercalated and exfoliated. Most of the time, an exfoliated structure is desired because of the excellent reinforcing efficiency of fully delaminated layered silicates.

Interestingly, layered clays (for example, sodium montmorillonite) can be converted into a lightweight, "house of cards"-like aerogel structure via the freeze-drying process. The production of montmorillonite clay aerogel was first reported by Mackenzie and Call [9, 10]. In 1967, Van Olphen [11] proposed that the edge-to-face conformation of particles within a clay aerogel, much like a "house of cards", occurred due to opposite edge and face electrostatic charges. The faces have a

negatively charged siloxane surface. The edges exhibit a positive charge because of the exposed alumina sheet. As a result, an edge-to-face type of association occurs due to the opposite charge attraction. The author also suggested that growing ice crystals push the clay particles aside, promoting parallel platelet alignment. Recently, Somlai, L.S. *et al.* [12] reported the synthesis of organically modified clay aerogels (OMCAS) from the freeze-drying of low viscosity surfactant-modified clay/water suspensions. The authors studied the effects of clay/water ratio, surfactants, and process parameters on aerogel structure. A lower concentration of clay, low shear force, slow rate of freeze-drying, or a less purified surfactant inhibit the occurrence of the aerogel structure, resulting in expanded powders instead of an aerogel structure. Composites using a hydrophilic clay aerogel as the nano-structured filler have been reported by a few researchers [13, 14]. Bandi, S.A. *et al.* [13] found that the physical encapsulation of clay aerogel within cross-linked PNIPAM polymer preserved the LCST behavior of the polymer with no breakdown in the structure through many cycles and enhanced its mechanical strength in its hydrogel form. The same authors reported that clay aerogel also enhanced the interfacial interaction with PVOH due to effective surface nucleation at low concentration and increased free volume at higher concentration, similar to those of the clay/PVOH composite [14]. However, a hydrophilic clay aerogel-filled natural rubber-based nanocomposite has so far not been studied.

In this work, we prepare NR-based nanocomposites via a new approach, the so-called "freeze-drying" process. Although this unique method allows the use of a limited amount of pure Na-MMT to incorporate into the NR latex, exfoliated nanocomposites are easily obtained without requiring any intercalating agents for improving the hydrophobicity of the pristine clay. An X-ray fluorescence spectrometer and a UV/vis spectrophotometer are used to characterize the elemental composition of the pristine clay, since the clay minerals have been often used as heterogeneous catalysts for promoting oxidative reactions, especially when they possess transition metal ions associated or structurally included with them—for instance, by the treatment of iron-rich smectites with Fe^{3+} and Al^{3+} chloride solutions, an effective catalyst for the hydroxylation of phenol was observed [15]. In addition, this present work involves the characterizations of the thermal- and

microwave-cured NR/clay aerogel nanocomposites and studies the effect of clay content on the cure characteristics and thermal stability of the nanocomposites as well. Finally, the influence of iron species present in Na-MMT clay on the thermal stability of NR is discussed.

4.3 Experimental Parts

4.3.1 Raw Materials

Natural rubber latex with 60% dry rubber content was kindly supplied by the Rubber Research Institute (Thailand). Vulcanization ingredients were purchased from the Rubber Research Center, Kasetsart University (Thailand). Pristine sodium montmorillonite (Na-MMT), with a cation exchange capacity (CEC) of 115 meq/100g and a particle size of < 45 μm, was kindly supplied by Kunimine Industries Co., Ltd., Tokyo, Japan.

4.3.2 Preparation of NR/Clay Aerogel Nanocomposites

A conventional (CV) formulation was used for preparing the prevulcanized NR latex. The latex was mixed with the vulcanization ingredients listed in Table 4.1 along with continuous stirring by a homogenizer at 70°C for 30 min. Then, the prevulcanized NR latex was kept in tight plastic bottles until use. To prepare the nanocompounds, a 1 wt% dispersion of pristine clay was added into the prevulcanized NR latex in various amounts with vigorous stirring for 2 h, followed by homogenizing stirring for 30 min at room temperature to ensure good mixing of the compounds. The coarse particles were filtered out, resulting in nanocompounds—which were checked for viscosity by using a Brookfield viscometer (Model: DV III). Then, the nanocompounds were immediately frozen within cylindrical glass shells at the temperature of liquid nitrogen. After freezing, the shells were attached to a lyophilizer (freeze-dryer) maintained at -54°C in a vacuum of less than 400 mtorr. This process usually took 36 h to entirely sublime the ice out: and NR/clay aerogel nanocomposites (Fig. 4.1) were ultimately obtained. The control for these samples was the prevulcanized NR latex. For the sample code.

NR stands for prevulcanized NR latex. and NR/xMMT stands for the nanocomposites, in which x indicates the weight percentage of pristine clay (phr).

4.3.3 Vulcanization Methods

In this work, two vulcanization methods were used: (1) thermal curing and (2) microwave curing. For the thermal method. the samples were cured in an oven at 100°C in order to preserve the white color of the vulcanizates. The cure time was fixed at 20 min [16]. For the microwave method. the samples were cured in a microwave oven—power: 100–850 W; wavelength: 12.24 cm; frequency: 2450 MHz; and magitron: OM75P(31)— under the same vulcanization temperature as the thermal curing. To achieve the optimum conditions, trial and error experiments were done; an infrared heat sensor gun was used for detecting the temperature of the chamber immediately after stopping the irradiation at a particular power and time. The results indicated that irradiation with a power of 450 W for 3 min gave a vulcanization temperature of 100°C. It should be noted that a longer cure time might cause overcuring of the samples.

4.3.4. Characterizations

4.3.4.1 X-Ray Fluorescence Spectrometer

Elemental analysis of the pristine clay and the nanocomposites was carried out by X-ray fluorescence using an Oxford Model ED2000. The excitation source was an X-ray tube with thin silver as the primary filter, operating at a tube voltage of 35 kV.

4.3.4.2 UV/Vis Spectrophotometer

The absorbance spectra of a 1 wt% clay aqueous suspension in distilled water and 0.4M H_2SO_4 were recorded on a UV/vis spectrophotometer 2550 (Shimadzu) scanning in the range of 200–600 nm at room temperature. Experiments were performed in a 1 cm quartz cuvette.

4.3.4.3 Brookfield Viscometer

The viscosity measurement of the nanocompounds was carried out with a Brookfield viscometer, Model RVDV-III. The experiments were performed by varying the size and speed of the spindle in order to achieve a shear stress close to 100%. Then, the viscosity data were collected. Shear rate and shear stress can be calculated by using the following equations:

$$\dot{\gamma} = \frac{2\omega(R_c)^2(R_b)^2}{\chi^2(R_c^2 - R_b^2)} \quad , \tag{4.1}$$

$$\tau = \eta \cdot \dot{\gamma} \quad , \tag{4.2}$$

where $\dot{\gamma}$ is the shear rate, ω is the angular velocity of the spindle, R_c and R_b are the radii of the container and the spindle, respectively, χ is the radius at which shear rate is calculated (normally the same value as R_b), and η and τ are viscosity and shear stress, respectively.

4.3.4.4 X-Ray Diffraction

X-ray diffraction patterns were taken with an X-ray diffractometer, Bruker AXS Model D8 Discover. The X-ray beam was Ni-filtered Cu Kα (λ = 0.154 nm), and the radiation operated at a tube voltage of 40 kV and a tube current of 40 mA. The samples were scanned in a step mode at a scan rate of 1.5°/min from 2θ = 1–20°. The interlayer spacing (d_{001}-spacing) was calculated via the Bragg equation:

$$\lambda = 2d\sin\theta \quad , \tag{4.3}$$

where λ is the X-ray wavelength, d is the interlayer spacing, and θ is the diffraction angle.

4.3.4.5 Scanning Electron Microscopy

The morphology was determined using a scanning electron microscope (JEOL, Model JSM5200). The samples were fractured in a liquid nitrogen bath and coated with gold under vacuum. All SEM digitized photographs were taken at an acceleration voltage of 15 keV with a magnification range between 75 and 2000x.

4.3.4.6 Hardness

Hardness was determined by a Shore A durometer according to ASTM D-2240. Five determinations of hardness at five different positions on the specimen were taken and averaged.

4.3.4.7 Cure Characteristics

The curing behavior was investigated at 150, 160, 170, and 180°C using a Monsato moving die rheometer (MDR2000) (Rubber Research Center, Kasetsart University, Thailand), operating at a 0.5° arc.

4.3.4.8 Crosslink Density Measurement

The crosslink densities of the vulcanizates from both methods were determined using a toluene-swelling method, as prescribed in ASTM D-6814-02. The vulcanizate samples were cut into squares (1 cm wide and 3–5 mm thick) and weighed before being swollen in toluene until equilibrium swelling, which normally took 72 h. The crosslink density was calculated by using the Flory–Rehner equation:

$$\nu_e = \rho_d / M_c = - [\ln(1-V_r) + V_r + \chi_1 V_r^2]/[V_1(V_r^{1/3}-V_r/2)] \quad , (4.4)$$

where M_c is the average molecular weight between the network crosslinks, ν_e is the network chain density (mol/cm^3), V_r is a volume fraction of rubber in a swollen network, V_1 is the molar volume of toluene (106.3 cm^3/mol), and χ_1 is the Flory–Huggins interaction parameter between toluene and polymer (0.391):

$$V_r = [(W_d - W_f)/\rho_d] / [((W_d - W_f)/\rho_d) + (W_s/\rho_s)] \quad , \qquad (4.5)$$

where W_d and W_s are the weight of dry rubber and the weight of solvent adsorbed by the sample, respectively, W_f is the weight of the filler in the sample, ρ_d is the density of the rubber compound, and ρ_s is the density of toluene (0.867 g/cm^3).

4.3.4.9 Differential Scanning Calorimetry (DSC)

DSC measurements were carried out with a NETZSCH differential scanning calorimeter model DSC 204 F1. The weight of the uncured and cured samples was in the range of 5–10 mg. The thermal scan was performed from 30°C to 250°C at a heating rate of 10°C/min under nitrogen atmosphere to determine

the vulcanization behavior of the uncured and cured composites. The heat of vulcanization was calculated by integrating the area under the exothermic signal.

4.3.4.10 Thermogravimetric Analysis (TG/DTA)

A Perkin-Elmer Pyris Diamond TG/DTA was used for determining the thermal stability of the composites. The weight of the samples was in the range of 15–20 mg. The samples were heated at a heating rate of 10°C/min from 30°C to 600°C in a nitrogen atmosphere.

4.4 Results and Discussion

4.4.1 Viscosity of Nanocompounds

Table 4.2 shows that the shear stress and viscosity of the latices increase as a function of clay content. The increment in both values indicates the high interaction and the formation of the network structure between the clay and the rubber. As described by Stephen, R. *et al.* [17], a more uniform distribution of clay particles, greater reinforcement of layered silicates, and the formation of a network structure between the clay and rubber are responsible for the enhancement in viscosity. Moreover, thixotropic behavior (i.e. viscosity gradually decreases at a particular shear rate along with time) is observed for all nanocompounds. This is due to the breakdown of network structure along with applied shear force.

4.4.2 Dispersion of Clay and Morphology of the Nanocomposites

Figure 4.2 shows the XRD patterns of Na-MMT and Na-MMT aerogel. The Na-MMT shows a diffraction peak at 2θ = 7.07°, corresponding to a d_{001}-spacing of 1.25 nm [18], whereas the Na-MMT clay aerogel exhibits a diffraction peak at 2θ = 6.99°, corresponding to a d_{001}-spacing of 1.26 nm. It appears that the change in d_{001}-spacing is not significant after converting to clay aerogel. As described by Bandi, S.A. [19], the clay aerogel is not an exfoliated structure (~10–12 Å thick), but instead appears as clay bundles (200 nm thick) held together via hydrated cations and as the rearrangement of these bundles through ice. Therefore, this might be the reason for the slight change in the d_{001}-spacing between pristine

clay and the clay aerogel. Figure 4.3 shows the XRD patterns of nanocomposites with various contents of Na-MMT. For nanocomposites with 1 and 2 phr Na-MMT, the shift in position of diffraction peak to a lower angle is clearly observed. NR/1MMT and NR/2MMT show a diffraction peak at 2θ = 4.04° and 2θ = 4.23° which corresponds to a d_{001}-spacing of 2.18 and 2.09 nm, respectively. The increase in d_{001}-spacing confirms the presence of rubber intercalation within the clay platelets, giving rise to an intercalated structure. In the case of the 3 phr-filled nanocomposite, no diffraction peak is observed, which indicates the extensive separation of clay platelets within the NR matrix, giving rise to an exfoliated structure.

An SEM micrograph of the Na-MMT powder is shown in Fig. 4.4a. Clearly, the pristine Na-MMT has a granular appearance with a particle size in the micron order. Once freeze-dried, a nice rearrangement of clay bundles, or "house of cards" structure, is observed, as shown in Fig. 4.4b, with micron-scale in the lateral dimension and nano-scale in the thickness dimension. The presence of a void inside the Na-MMT aerogel structure after the sublimation of ice can be seen in Fig. 4.4c. Figure 4.5 shows SEM micrographs of NR (Fig. 4.5a) and its nanocomposites (Fig. 4.5b–d). In the case of 1 and 2 phr-filled nanocomposites, we deduce that there is not enough clay content for forming the aerogel structure; on the other hand, the micrograph of the NR/3MMT reveals that the aerogel structure begins to form. According to Bandi, S.A. [19], clay aerogel can be formed via two mechanisms: (1) gelation and (2) rearrangement through ice. In the gelation step, clay bundles are formed due to a high degree of swelling of the Na-MMT in water, followed by the electrostatic interaction between positively charged edges and negatively charged faces, resulting in edge-to-face conformation. Then, rearrangement of these bundles through ice occurs at the freezing step. It turns out that the 3 phr-filled nanocomposite has enough clay content for undergoing those mechanisms and forming the aerogel structure, while the others cannot. Based on the XRD and SEM results, it can be said that NR/3MMT not only provides the exfoliated structure but also gives the clay aerogel structure in some regions, as shown in Fig. 4.5e. Besides, the observed aerogel structure is totally encapsulated with NR (Fig. 4.5e). A similar observation was made by Bandi, S.A. *et al.* [13].

4.4.3 Hardness

Figure 4.6 shows the hardness of the freeze-dried NR and nanocomposites. The graph shows that hardness increases as a function of clay content in the following order: NR/3MMT > NR/2MMT > NR/1MMT > NR, as expected. Compared with NR, 1, 2, and 3 phr-filled nanocomposites provide increments of 45, 57, and 102% on the hardness value, respectively. It is noticeable that the Na-MMT clay behaves like a reinforcing agent for the rubber matrix and enhances the hardness of the composites.

4.4.4 Cure Characteristics

The cure characteristics of NR and its nanocomposites are listed in Table 4.3. To study the effect of temperature on the cure characteristics, different vulcanization temperatures were selected: 150, 160, 170, and 180°C. The results show that the cure time, denoted as t_{90}, decreases with an increase in vulcanization temperature in all compounds, as expected. This effect is attributed to the vulcanization rate enhancement as the vulcanization temperature increases, corresponding with earlier work [20]. To investigate the effect of clay on the cure characteristics, optimum cure time and maximum rheometric torque are focused on. Upon the incorporation of clay, the vulcanization reaction of nanocomposites is delayed, as indicated by the increase of cure times. This is explained by the interaction between the components of the cure system and the clay surface [21]. However, when performing at high vulcanization temperature (e.g. 180°C), this effect is negligible owing to the vulcanization rate enhancement. In addition, the nanocomposites exhibit a higher maximum rheometric torque (more stiffness) than pure NR, especially for NR/2MMT and NR/3MMT. Again, this is attributed to the reinforcing effect of clay and the good interaction between the clay and the rubber. Assuming this maximum rheometric torque is related to the crosslink density [20, 22, and 23], NR/3MMT should give the highest crosslink density. To prove this hypothesis, crosslink density measurement was performed. Additionally, a slight decrease in maximum rheometric torque at high vulcanization temperature for NR and its nanocomposites indicates that crosslink density decreases as vulcanization temperature increases [23]. This points to an overcuring reversion reaction in which

polysulfidic linkages undergo breakage at high vulcanization temperature; as a result, the maximum rheometric torque and crosslink density tend to decrease [20, 23].

The DSC measurements under non-isothermal conditions were performed in order to investigate the vulcanization behavior of the uncured composites, as revealed in Fig. 4.7, and the curing enthalpy is calculated via integrating the area under the exothermic signal. The DSC thermogram of NR shows onset and peak temperatures of curing at 170 and 186°C, respectively, whereas those of the nanocomposites are located at 173 and 190.3°C for NR/1MMT, 173 and 190.5°C for NR/2MMT, and 173 and 190.6°C for NR/3MMT, respectively. A slight increase in the onset and peak curing temperature of the nanocomposites is in accordance with the rheometer results; that is, there is an interaction between the components of the cure system and the clay surface, causing a delay in the vulcanization reaction. Furthermore, the heat evolved during the vulcanization reaction can be used to assess the amount of crosslinking of NR and its nanocomposites. As shown in Fig. 4.7, the curing energies are 2.2, 1.83, 1.68, and 1.48 J/g for NR, NR/1MMT, NR/2MMT, and NR/3MMT, respectively. The decrease in curing energies with the content of clay demonstrates the effect of Na-MMT clay on the vulcanization reaction; that is, the interfacial interaction between the layered silicates and the rubber matrix restricts the segmental motion of the rubber chains and changes the vulcanization rate. As a result, the amount of crosslinking of the nanocomposites is less than that of pure NR.

4.4.5 Crosslink Density Measurement

Table 4.4 summarizes the swelling ratio and calculated crosslink density of thermal- and microwave-cured vulcanizates. Regardless of the curing methods, the swelling ratio of the vulcanizates gradually decreases with increasing clay content from 1 to 3 phr, as expected. This can be ascribed to a uniform dispersion of the layered silicates, which further forms a physical crosslink with the rubber matrix and immobilizes the rubber chains [24], and thereby hinders the transportation of toluene to the vulcanizates. Nevertheless, it should be mentioned here that the effect of layered silicates on the amount of crosslinking, as indicated by a decrease in the curing energy obtained from the DSC thermograph with the

presence of clay, can be counterbalanced by the ability of the layered silicates to undergo a physical crosslink with the rubber matrix. As a result, the calculated crosslink density of pure NR increases with the addition of impermeable clay layers and reaches the maximum at the 3 phr-filled nanocomposite. These results support the above hypothesis in which more clay content leads to more crosslink density and more reinforcement in the rubber matrix [8]. When considering the effect of curing methods, it is found that thermal curing provides a higher crosslink density than microwave curing for pure NR and NR/1MMT. On the other hand, the reverse is observed for NR/2MMT and NR/3MMT. Since both curing methods were carried out at the same temperature, the mechanism of heat generation and heat distribution might be responsible for the differences in crosslink density of both methods. Normally, the curing of natural rubber is carried out with a conventional thermal cure, involving a direct heat transfer from an external heater to the sample. The problems of conventional thermal curing arise from the need for long curing time together with a large temperature gradient across the sample thickness. It turns out that microwave curing seems to be a more efficient method for curing natural rubber due to the faster curing time, more uniform heat distribution along the thickness during curing, and hence more uniform crosslinking [25, 26]. For pure NR and NR/1MMT, the thermal cure method seems to be independent of the heat conduction and convection effects; as a consequence, the crosslink density of thermal curing is higher than that of microwave curing. It is believed that 1 phr of Na-MMT clay does not inhibit the thermal curing of rubber. However, the effect of Na-MMT clay on the curing of composites is more pronounced for NR/2MMT and NR/3MMT. One can notice that microwave-cured NR/2MMT and NR/3MMT show higher crosslink densities than those of thermal curing, and this could be ascribed to the uniform heat distribution during microwave curing and more dependence on the heat conduction and convection effects of thermal-cured NR/2MMT and NR/3MMT.

To monitor the further vulcanization of NR and its nanocomposites after being cured by thermal and microwave methods, DSC measurements were carried out, as shown in Figs. 4.8 and 4.9. Surprisingly, an endothermic signal is observed instead of an exothermic signal, for all samples. The presence of the endothermic signal can be explained in terms of the thermally unstable polysulfidic

linkage upon exposure to heat, resulting in desulfuration to shorter linkages [23]. Assuming that the heat of reaction calculated from integrating the area under the endothermic signal is related to the fraction of polysulfidic linkage (Table 4.5), one can notice that microwave-cured vulcanizates give a higher polysulfidic linkage than thermal-cured vulcanizates—the same explanation (i.e. uniform heat distribution during microwave curing) as being given above in the crosslink density results. Furthermore, partially cured NR/2MMT via both curing methods shows the highest fraction of polysulfidic linkage compared with the others. From the above results, it is important to note that both curing methods have already provided fully-cured vulcanizates.

4.4.6 Thermogravimetric Analysis

Thermogravimetric analysis was used for studying the effect of Na-MMT clay on the thermal stability of the nanocomposites, and the results are shown in Fig. 4.10. The onset degradation and peak degradation temperatures of NR are 353.4 and 380.4°C, respectively. To our knowledge, the inorganic species (e.g. Na-MMT clay) have good thermal stability; hence, the incorporation of these species into organic matrices should improve their thermal stability. Surprisingly, it was found that both the onset and peak degradation temperatures of NR slightly decrease with an increase in Na-MMT clay content; those are 352.1 and 380.3°C for NR/1MMT, 349.1 and 376.3°C for NR/2MMT, and 348.5 and 375.5°C for NR/3MMT, respectively. This points to an acceleration in the thermal degradation of NR by ferric ion (Fe^{3+}) isomorphously substituted in the octahedral sheet of Na-MMT clay. The presence of an iron species in Na-MMT clay can be identified by elemental analysis (Tables 4.6 and 4.7). In addition, to ensure the existence of ferric ion in the octahedral sheet, UV/vis spectrophotometry was carried out as well. Figure 4.11 shows the absorbance spectra of a 1 wt% clay aqueous suspension in distilled water and 0.4M H_2SO_4. The appearance of a broad band at 242 and 244 nm points to the charge transportation from O^{2-}, OH^-, or H_2O to the iron (Fe^{3+}) in the octahedral layer of the clay mineral [27]. This certainly confirms that the ferric ions present in the Na-MMT clay are those from the octahedral sheet, and not from the contaminants, because, as Rao *et al.* stated, the basic structural SiO_4 units of

tetrahedral sheets in the clay lattice do not absorb light in the wavelength ranging from 200 to 800 nm, except when the transition metal ions in the silicate structure are exchanged. Transition metal cations (e.g. Fe^{3+} and Al^{3+}) appearing at both the crystal edges and the planar surfaces of smectite clay can act as an oxidizing agent (electron acceptor) [28]. This ability of clay is confirmed by testing with a benzidine solution. The transfer of an electron from benzidine to the clay changes benzidine from colorless to blue, as shown in Fig. 4.12. In our study, it is confirmed that Fe^{3+} exposed at the crystal edge would directly possess oxidizing sites for the NR. Considering the fact that the NR used in preparing the nanocomposites was prevulcanized NR latex, the double bond is still available for undergoing further reaction. During the TGA measurement, the ferric ion will activate the oxidation reaction of NR, which leads to the transfer of an electron from the double bond to the clay (Fig. 4.13); as a consequence, the thermal degradation of NR is accelerated, as observed via the decrease in onset and peak degradation temperatures. Besides, this effect is more pronounced for the 3 phr-filled nanocomposite. A similar observation has been reported by Morlat *et al.* [29]. They stated that the presence of iron cations beside magnesium within the octahedral sheet of Na-MMT clay catalyzed the degradation of polypropylene (PP), as indicated by a reduction in the length of the induction period in the photo-oxidation reaction of a PP/MMT nanocomposite.

4.5 Conclusions

Natural rubber latex/clay aerogel nanocomposites were successfully prepared by freeze-drying technique. Viscosity and shear stress of the nanocompounds increased upon the incorporation of clay due to the formation of a rubber–clay network. The thixotropic behavior was observed in all nanocompounds due to the breakdown of the network structure after encountering the shear force. XRD patterns indicated that an intercalated structure occurred in the 1 and 2 phr-filled nanocomposites, whereas an exfoliated structure occurred in the 3 phr-filled nanocomposite. SEM studies revealed that a clay aerogel structure was formed at the 3 phr clay loading. Upon the incorporation of clay, the enhancement of hardness, maximum rheometric torque (stiffness), and

crosslink density—compared with those of pure NR—signified the reinforcing effect of pristine clay in composites and a good interaction between the clay and the rubber. The crosslink density of the clay-filled NR vulcanizates increased with the pristine clay content in both thermal and microwave curing methods. Considering the effect of both curing methods, thermal curing provided a higher crosslink density than microwave curing for pure NR and NR/1MMT, while NR/2MMT and NR/3MMT showed the reverse. It was also found that NR/2MMT contained the highest fraction of polysulfidic linkage due to the highest area under the endothermic signal. TGA studies indicated that pristine clay accelerated the decomposition of NR, showing a decrease in onset and decomposition temperatures. This is associated with an acceleration in the thermal degradation of NR by the ferric ion present at the octahedral sheet of smectite clay.

4.6 Acknowledgements

The authors would like to thank the Thailand Research Fund through the Royal Golden Jubilee Ph.D. Program (PHD/0088/2549) for providing financial support. The authors are also grateful to Assoc. Prof. David A. Schiraldi for providing helpful discussions.

4.7 References

1. Teh PL, Mohd Ishak ZA, Hashim AS, Karger-Kocsis J, Ishiaku US. Effects of epoxidized natural rubber as a compatibilizer in melt compounded natural rubber-organoclay nanocomposites. European Polymer Journal 2004;40:2513-2521.
2. Wang Y, Zhang L, Tang C, Yu D. Preparation and characterization of rubber-clay nanocomposites. Journal of Applied Polymer Science 2000;78:1879-1883.
3. Wang Y, Zhang H, Wu Y, Yang J, Zhang L. Structure and properties of strain-induced crystallization rubber-clay nanocomposites by co-coagulating

the rubber latex and clay aqueous suspension. Journal of Applied Polymer Science 2005;96:318-323.

4. Wu YP, Wang YQ, Zhang HF, Wang YZ, Yu DS, Zhang LQ, Yang J. Rubber-pristine clay nanocomposites prepared by co-coagulating rubber latex and clay aqueous suspension. Composites Science and Technology 2005;65:1195-1202.
5. Wang Y, Zhang H, Wu Y, Yang J, Zhang L. Preparation and properties of natural rubber/rectorite nanocomposites. European Polymer Journal 2005;41:2776-2783.
6. Sharif J, Wan Md Zin Wan Yunus, Khairul Zaman Hj Mohd Dahlan, Mansor Hj Ahmad. Preparation and properties of radiation crosslinked natural rubber/clay nanocomposites. Polymer Testing 2005;24:211-217.
7. Valadares LF, Leite CAP, Galembeck F. Preparation of natural rubber-montmorillonite nanocomposite in aqueous medium: evidence for polymer-platelet adhesion. Polymer 2006;47:672-678.
8. Stephen R, Ranganathaiah C, Varghese S, Joseph K, Thomas S. Gas transport through nano and micro composites of natural rubber (NR) and their blends with carboxylated styrene butadiene rubber (XSBR) latex membranes. Polymer 2006;47:858-870.
9. Mackenzie RC. Clay-water relationships. Nature 1952;171:681-683.
10. Call F. Preparation of dry clay-gels by freeze-drying. Nature 1953;172:126.
11. Van Olphen H. Polyelectrolyte reinforced aerogels of clays-application as chromatographic adsorbents. Clay Miner.1967;15:423-435.
12. Somlai LS, Bandi SA, Schiraldi DA. Facile processing of clays into organically-modified aerogels. AIChE Journal 2006;52(3):1-7.
13. Bandi SA, Bell M, Schiraldi DA. Temperature-responsive clay aerogel-polymer composites. Macromolecules 2005:38:9216-9220.
14. Bandi SA, Schiraldi DA. Glass transition behavior of clay aerogel/poly(vinyl alcohol) composites. Macromolecules 2006;39:6537-6545.
15. Letaïef S, Casal B, Aranda P, Martin-Luengo MA, Ruiz-Hitzky E. Fe-containing pillared clays as catalysts for phenol hydroxylation 2003;22:263-277.

16. Travas-Sejdic J, Jelencic J, Bravar M, Frobe Z. Characterization of the natural rubber vulcanizates obtained by different accelerators. European Polymer Journal 1996;32(12):1395-1401.

17. Stephen R, Alex R, Cherian T, Varghese S, Joseph K, Thomas S. Rheological behavior of nanocomposites of natural rubber and carboxylated styrene butadiene rubber latices and their blends. Journal of Applied Polymer Science 2006;101:2355-2362.

18. Dong W, Zhang X, Liu Y, Gui H, Wang Q, Gao J, Song Z, Lai J, Huang F, Qiao J. Effect of rubber on properties of nylon-6/unmodified clay/rubber nanocomposites. European Polymer Journal 2006;42:2515-2522.

19. Bandi SA. Unpublished Ph.D. Dissertation, Case Western Reserve University, Cleveland, Ohio.

20. López-Manchado MA, Arroyo M, Herrero B, Biagiotti J. Vulcanization kinetics of natural rubber-organoclay nanocomposites. Journal of Applied Polymer Science 2003;89:1-15.

21. Arroyo M, López-Manchado MA, Valentín JL, Carretero J. Morphology/behavior relationship of nanocomposites based on natural rubber/epoxidized natural rubber blends. Composites Science and Technology 2007;67:1330-1339.

22. Arroyo M, López-Manchado MA, Herrero B. Organo-montmorillonite as substitute of carbon black in natural rubber compounds. Polymer 2003;44:2447-2453.

23. Kurian T, George KE, Francis DJ. Effect of vulcanization temperature on the cure characteristics and vulcanizate properties of natural rubber and styrene-butadiene rubber. Die Angewandte Makromolekulare Chemie 1988;162:123-134.

24. Kader MA, Kim K, Lee YS, Nah C. Preparation and properties of nitrile rubber/montmorillonite nanocomposites via latex blending. J Mater Sci 2006;41:7341-7352.

25. Sombatsompop N, Kumnuantip C. Comparison of physical and mechanical properties of NR/carbon black/reclaimed rubber blends vulcanized by

conventional thermal and microwave irradiation methods. Journal of Applied Polymer Science 2006;100:5039-5048.

26. Chaowasakoo T, Sombatsompop N. Mechanical and morphological properties of fly ash/epoxy composites using conventional thermal and microwave curing methods. Composites Science and Technology 2007;67:2282-2291.

27. Rao GR, Mishra BG. A comparative UV-vis-diffuse reflectance study on the location and interaction of cerium ions in Al- and Zr-pillared montmorillonite clays. Materials Chemistry and Physics 2005;89:110-115.

28. Theng BKG. Mechanisms of formation of colored clay-organic complexes. Clays and Clay Minerals 1971;19:383-390.

29. Morlat S, Mailhot B, Gonzalez D, Gardette JL. Photo-oxidation of polypropylene/montmorillonite nanocomposites. 1. Influence of nanoclay and compatibilizing agent. Chem. Mater.2004;16:377-383.

Table 4.1 Formulation of the rubber compound

Ingredients	Dry (parts by weight)	Wet (parts by weight)
60 % Natural rubber latex	100.0	166.67
10 % Potassium hydroxide solution	0.5	5.0
50 % Zinc oxide dispersion	1.0	2.0
50 % Calcium carbonate dispersion	10.0	20.0
50 % Sulfur dispersion	1.0	2.0
50 % ZDEC[a] dispersion	0.75	1.5
50 % Wingstay-L[b] dispersion	1.0	2.0
1 % Clay dispersion	1.0, 2.0, 3.0	100.0, 200.0, 300.0

[a] Zinc diethyl dithiocarbamate (ZDEC).

[b] Wingstay-L, antioxidant.

Table 4.2 Viscosity measurement of different rubber compounds

Materials	Shear rate (1/s)	Shear stress (Pa)	Viscosity (mPas)
NR [a]	54.64	3.61	66.10
NR/1MMT [a]	47.21	3.58	75.95
NR/2MMT [b]	32.04	11.82	369.00
NR/3MMT [b]	0.93	12.00	12,877.00

[a] carried out with spindle 01.

[b] carried out with spindle 02.

[a, b] carried out with a Brookfield viscometer at a temperature of 27°C.

Table 4.3 Curing characteristics of NR and its composites

Materials	T_c (°C)[a]	ts_2 (min)[b]	t_{90} (min)[c]	S_{max} (dNm)[d]	S_{min} (dNm)[e]	ΔS (dNm)[f]
NR	150	0.30	12.51	3.33	1.64	1.69
	160	0.30	5.01	3.24	1.27	1.97
	170	0.30	2.37	3.15	1.34	1.81
	180	0.30	1.28	3.18	1.55	1.63
NR/1MMT	150	0.30	14.07	3.63	1.74	1.89
	160	0.60	6.39	3.36	2.18	1.18
	170	0.30	3.06	3.25	1.95	1.30
	180	0.30	1.37	3.14	1.96	1.18
NR/2MMT	150	0.30	18.31	4.52	2.78	1.74
	160	0.30	5.58	4.63	1.81	2.82
	170	0.20	3.10	4.34	2.26	2.08
	180	0.30	1.21	4.23	0.86	3.37
NR/3MMT	150	0.30	16.38	5.03	2.67	2.36
	160	1.00	8.00	5.86	4.19	1.67
	170	0.30	3.20	5.24	2.87	2.37
	180	1.00	1.20	4.65	3.6	1.05

[a] vulcanization temperature.

[b] scorch time.

[c] optimum cure time.

[d] maximum rheometric torque.

[e] minimum rheometric torque.

[f] the difference between maximum and minimum torque.

Table 4.4 Swelling ratios and calculated crosslink densities (v_e) of the thermal-and microwave-cured vulcanizates

Materials	Thermal curing		Microwave curing	
	Swelling ratio*	v_e [mol/cm^3]	Swelling ratio*	v_e [mol/cm^3]
NR	23.98	$3.51 * 10^{-6}$	28.69	$2.43 * 10^{-6}$
NR/1MMT	22.60	$3.57 * 10^{-6}$	27.76	$3.14 * 10^{-6}$
NR/2MMT	21.02	$3.65 * 10^{-6}$	17.60	$4.56 * 10^{-6}$
NR/3MMT	17.32	$5.08 * 10^{-6}$	15.48	$5.66 * 10^{-6}$

*Swelling ratio is calculated using the following equation:

Swelling ratio $= \frac{(w_2 - w_1)}{w_1}$, where w_2 and w_1 are the weight of swollen rubber and dry rubber, respectively.

Table 4.5 Heat of reaction (ΔH) of partially-cured vulcanizates involving further vulcanization reaction

Materials		ΔH (J/g)
Thermal-cured	NR	-14.44
	NR/1MMT	-13.77
	NR/2MMT	-28.05
	NR/3MMT	-13.04
Microwave-cured	NR	-31.62
	NR/1MMT	-21.40
	NR/2MMT	-40.29
	NR/3MMT	-26.78

Table 4.6 Elemental analysis of Na-MMT

Al	Si	S	K	Ca	Ti	Fe	Cu	Zn	Sr	Y	Zr
1.22[a]	7.27[a]	1286[b]	675 [b]	0.39[a]	1165[b]	1.39[a]	62[b]	53[b]	59[b]	10[b]	45[b]

Table 4.7 Elemental analysis of NR/3MMT

Si	P	S	K	Ca	Ti	Fe	Cu	Zn
0.92[a]	800[b]	1.38[a]	1.28[a]	2.7[a]	158[b]	1445[b]	552[b]	6.34[a]

[a] wt%

[b] ppm.

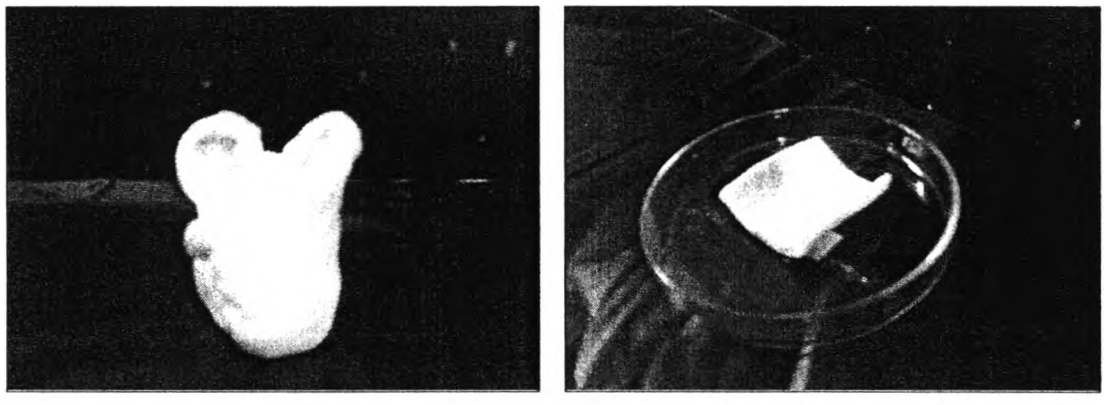

(a) (b)

Figure 4.1 Photographs of NR/clay aerogel nanocomposites: (a) NR/1MMT and (b) NR/2MMT.

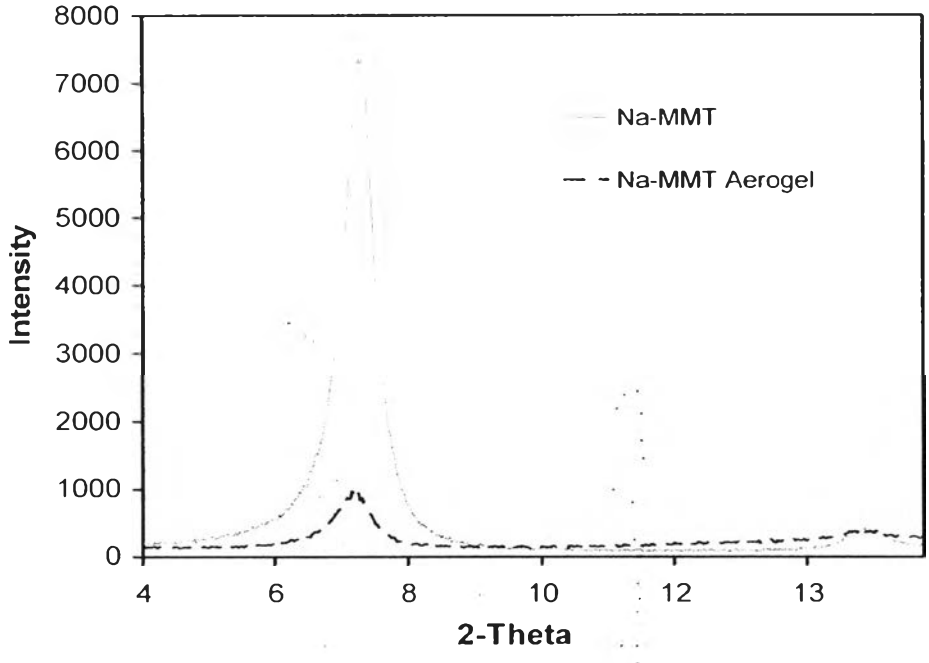

Figure 4.2 XRD patterns of Na-MMT and Na-MMT aerogel.

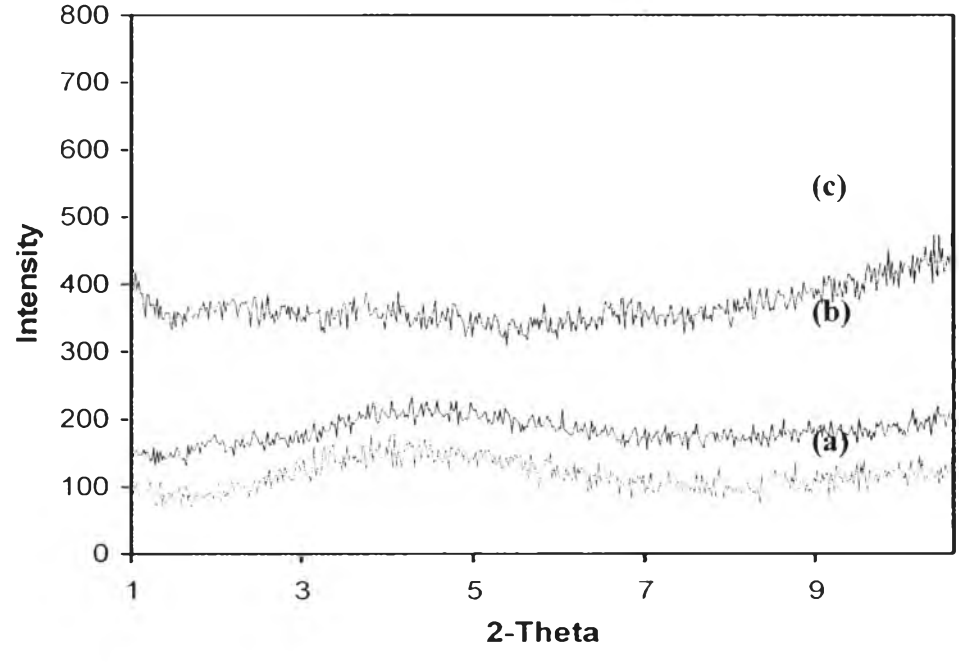

Figure 4.3 XRD patterns of (a) NR/1MMT, (b) NR/2MMT, and (c) NR/3MMT nanocomposites.

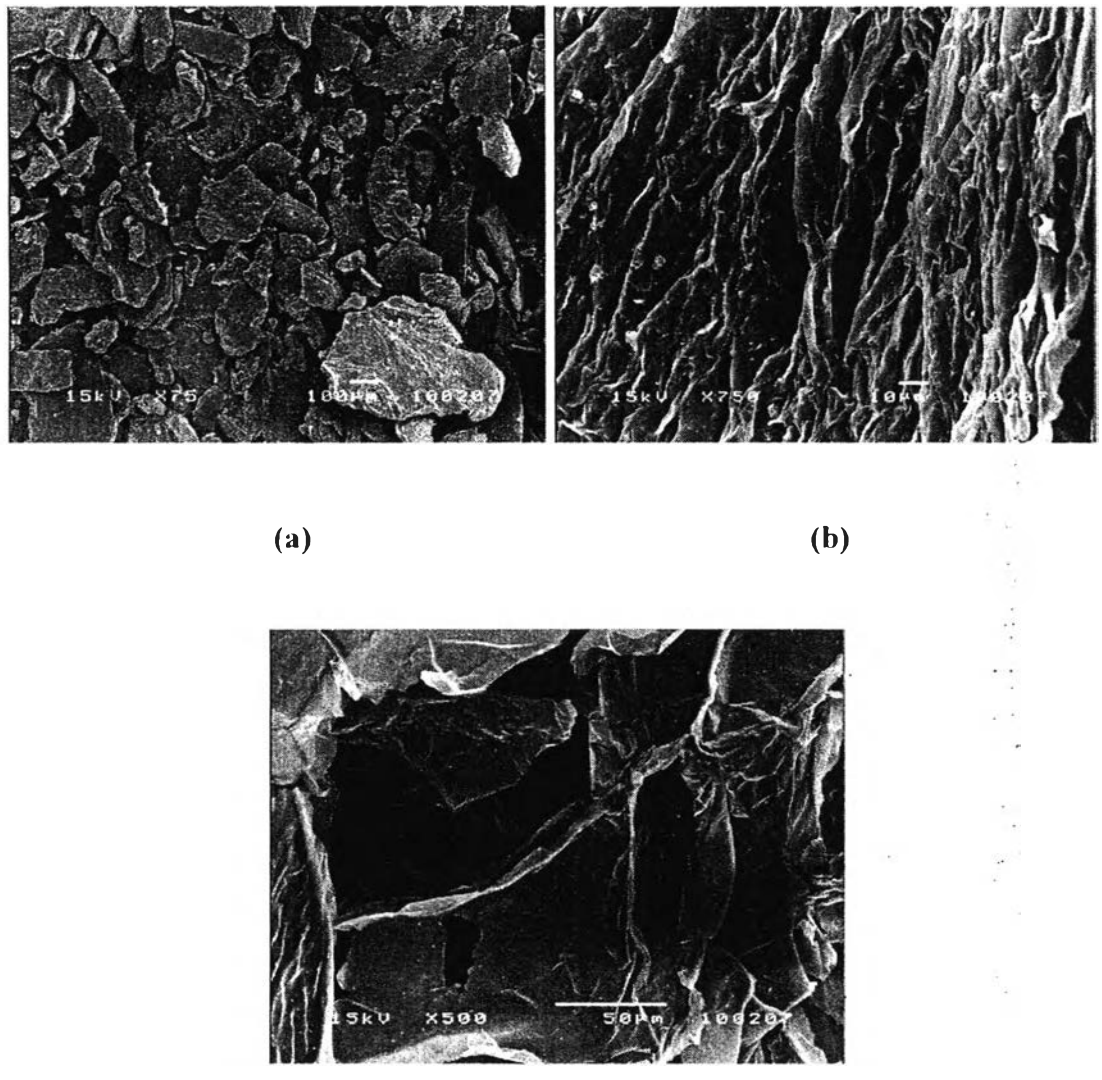

(a) **(b)**

(c)

Figure 4.4 SEM micrographs of (a) Na-MMT, (b) Na-MMT aerogel structure, and (c) the void inside the Na-MMT aerogel after the sublimation of ice.

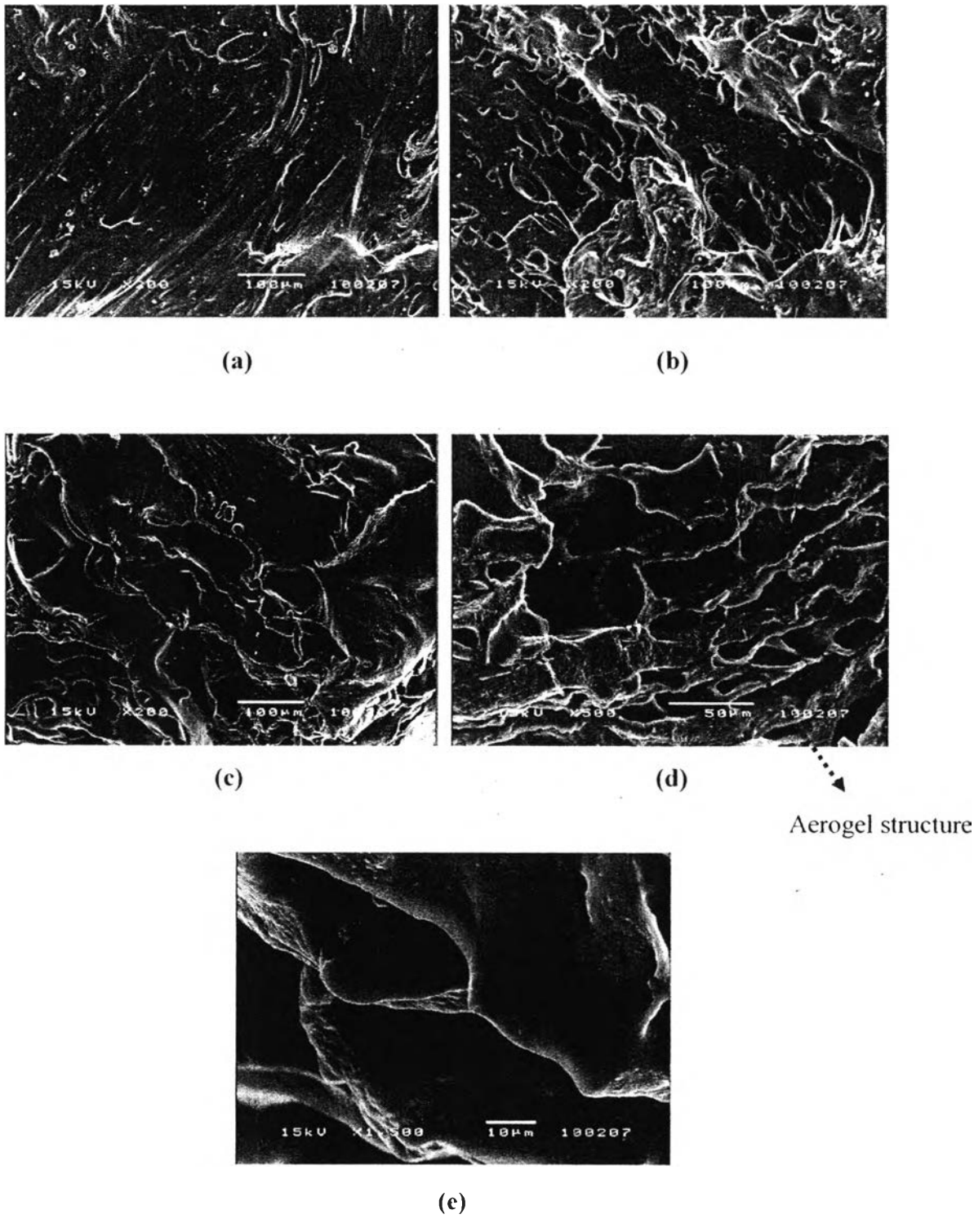

Figure 4.5 SEM micrographs of (a) NR, (b) NR/1MMT, (c) NR/2MMT, (d) NR/3MMT, and (e) NR/3MMT at higher magnification.

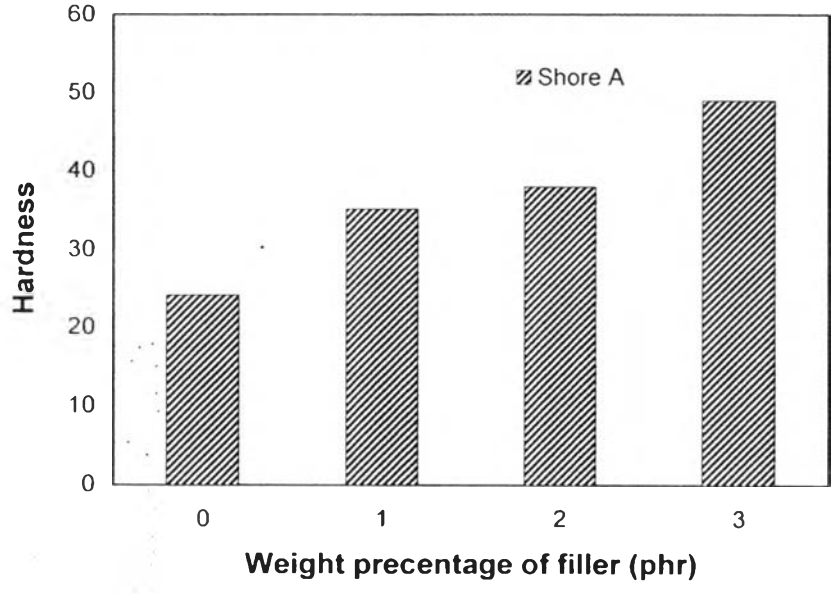

Figure 4.6 Hardness results of freeze-dried NR and nanocomposites.

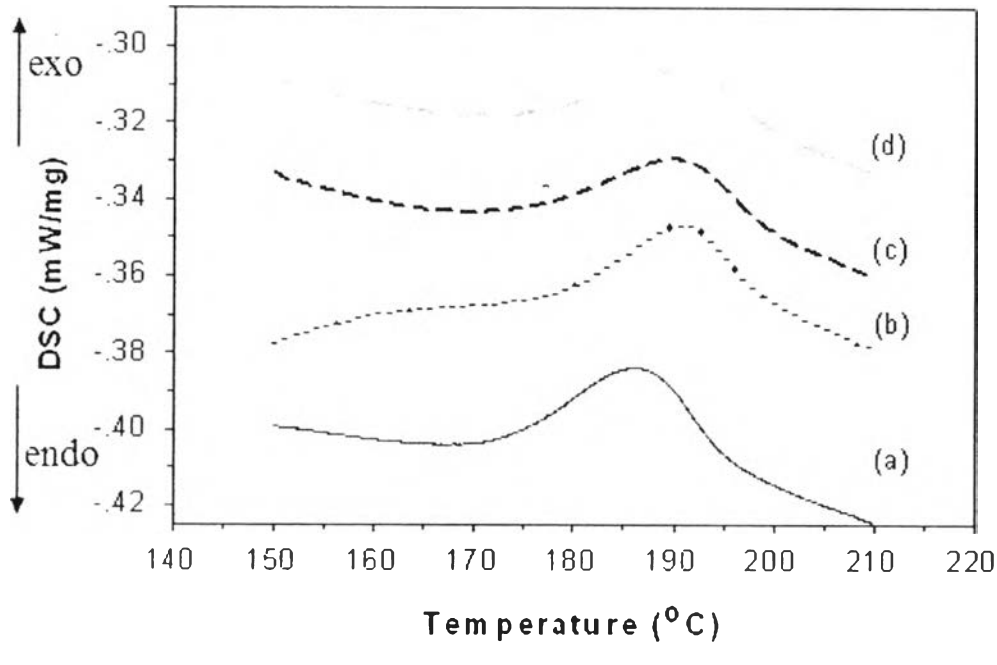

Figure 4.7 DSC thermograms of uncured (a) NR, (b) NR/1MMT, (c) NR/2MMT, and (d) NR/3MMT.

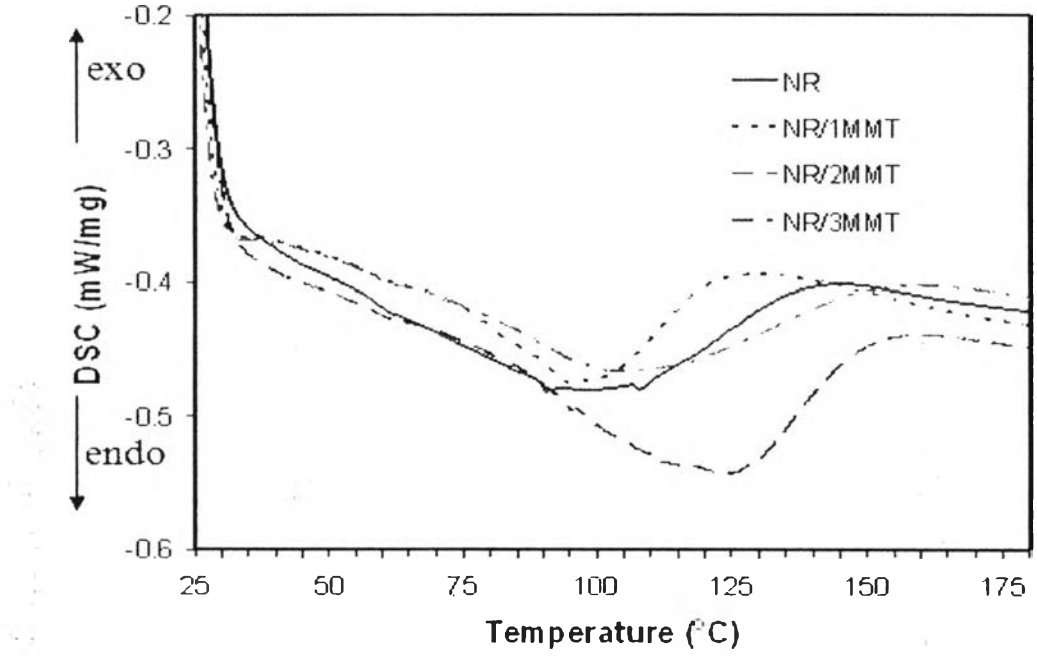

Figure 4.8 DSC thermograms of NR and its nanocomposites after microwave curing.

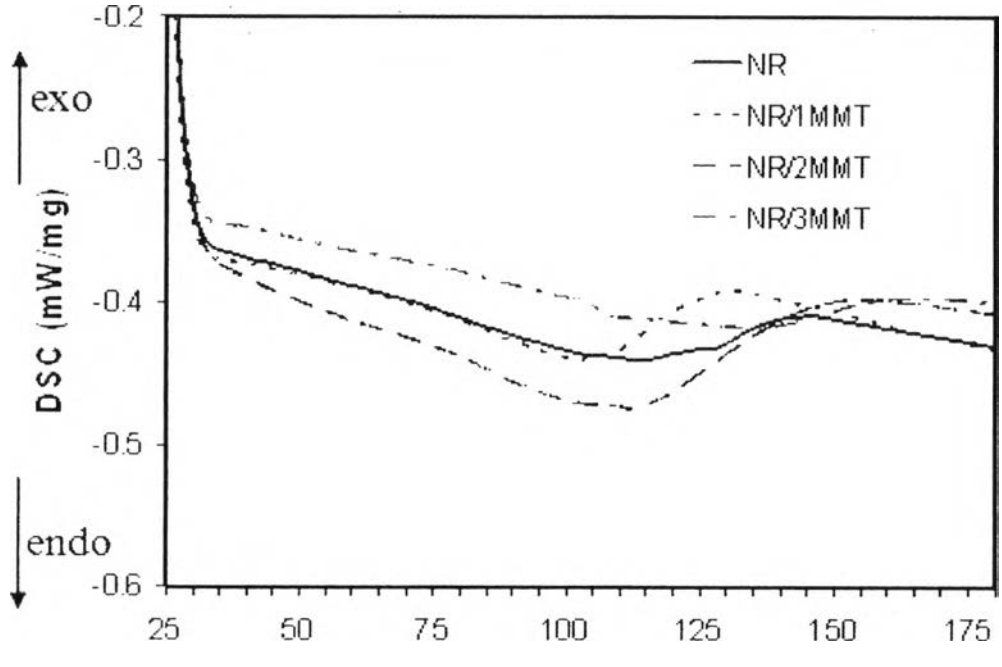

Figure 4.9 DSC thermograms of NR and its nanocomposites after thermal curing.

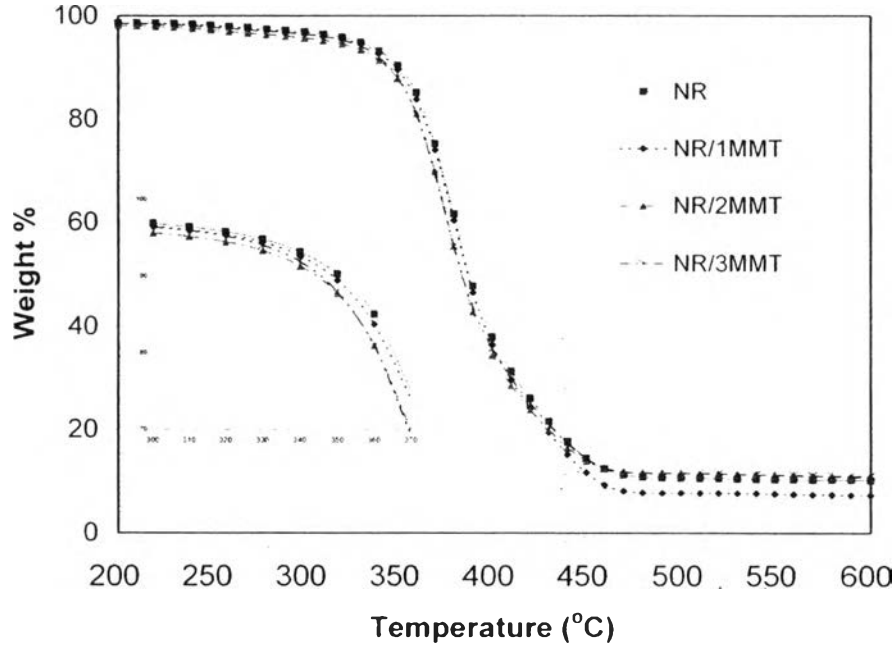

Figure 4.10 TGA results of NR and its nanocomposites.

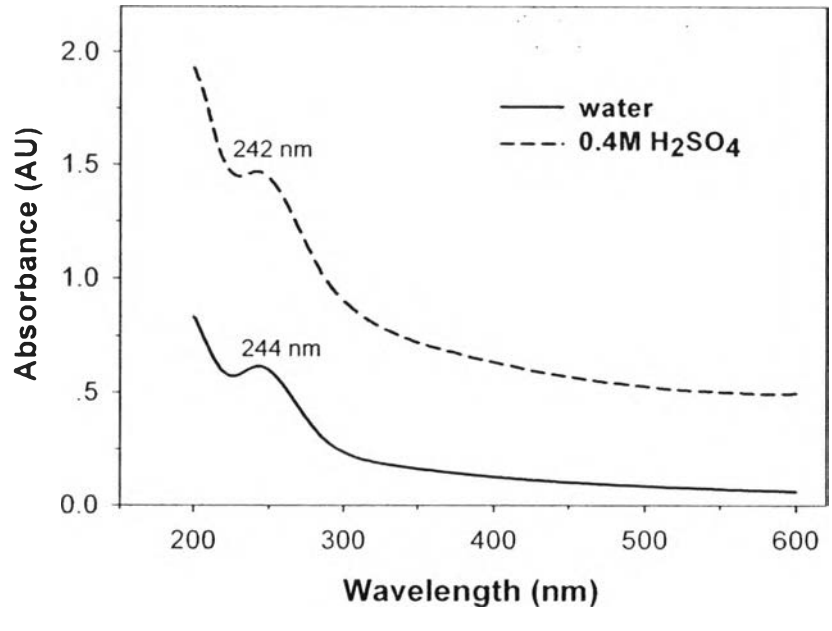

Figure 4.11 The UV/vis absorbance spectra of a 1 wt% clay aqueous suspension in (a) distilled water and (b) 0.4M H_2SO_4.

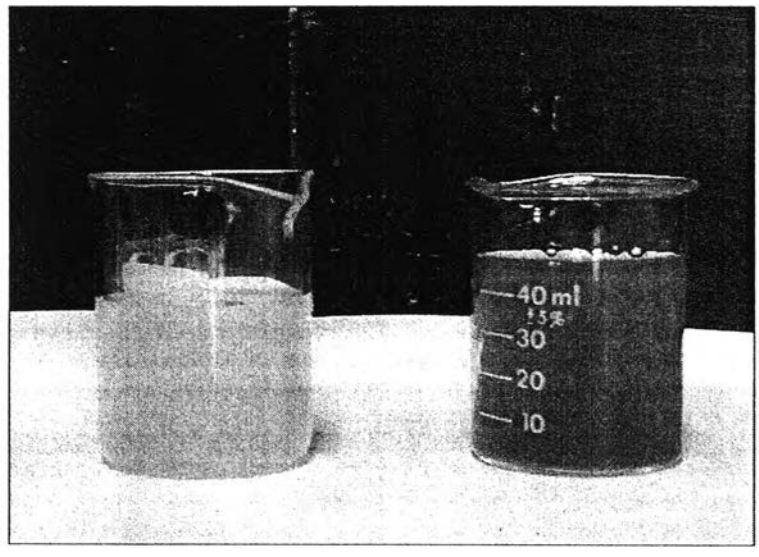

Figure 4.12 Physical comparison between (a) starting clay solution and (b) clay solution after testing with benzidine.

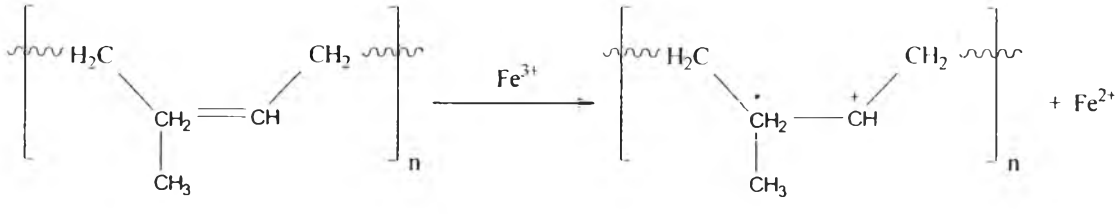

Figure 4.13 Mechanism of thermal degradation of NR in the presence of ferric ion.